Prediction of Fracture Toughness of Metallic Materials

Fuzuli Ağrı Akçay[1,2,*], Erkan Oterkus[3]

1 İstanbul Teknik Üniversitesi Gemi İnşaatı ve Deniz Bilimleri Fakültesi, Maslak, İstanbul 34469, Turkey.

2 Department of Mechanical and Aerospace Engineering, University of Central Florida, 4000 Central Florida Blvd., Orlando, FL 32816, USA.

3 Department of Naval Architecture, Ocean and Marine Engineering, University of Strathclyde, Glasgow G4 0LZ, UK.

*Corresponding author: Fuzuli Ağrı Akçay: akcayfu@itu.edu.tr

ABSTRACT

Fracture toughness is a measurement of fracture resistance and is a crucial parameter in designing and manufacturing structural engineering components, including the components of ships and offshore structures. However, accurate measurement of fracture toughness requires a fatigue pre-cracked specimen which can be challenging to prepare in extremely brittle materials. Moreover, specimen thickness is another requirement which can be challenging to achieve as well, particularly in very tough materials. Therefore, a physics-based closed-form analytical expression is proposed to determine fracture toughness of isotropic materials simply by utilizing a uniaxial tensile test specimen. The expression naturally introduces a length scale parameter, consistent with non-local applications, such as peridynamics, as well. Fracture toughness of various metallic materials, including both brittle and ductile, are predicted and compared to the experimental results in the literature. Predicted fracture toughness values are in good agreement with the experimentally measured ones.

Keywords: Fracture toughness; Length scale; Metallic materials; Strength; Non-local

Nomenclature

A	area of the fracture plane
C_I	specific surface energy density (of Mode I fracture)
de_I, de_{II}, de_{III}	elastic strain increments of the unfractured medium in principal directions
dW	mechanical work increment of the unfractured medium
dW^*	mechanical work increment of the fractured medium
e_I	elastic strain in the first principal direction
E	Young's modulus
K_{Ic}	plane strain fracture toughness (of Mode I)
$l_{I,0}$	characteristic length (relevant to fracture process)
l_I, l_{II}, l_{III}	current dimensions of the volume element in principal directions
x_0	atomic spacing (at equilibrium)
σ_{cs}	theoretical cohesive strength
$\sigma_I, \sigma_{II}, \sigma_{III}$	principal stresses of the unfractured medium
$\sigma_I^*, \sigma_{II}^*, \sigma_{III}^*$	principal stresses of the fractured medium
σ_{Ic}	critical (tensile) stress at fracture
σ_y	yield strength
υ	Poisson's ratio
γ_s	surface energy per unit area
Γ_I	critical effective energy release rate (of Mode I fracture)

1. Introduction

Accurate prediction of material failure is of great significance for designing and manufacturing engineering structures as their failure may cause not only economic loss but also loss of human life. Material failure can be divided into two categories as brittle fracture and ductile fracture. Brittle fracture addresses failures that cause an abrupt loss in the load carrying capability of the structure, whereas ductile fracture is associated to large plastic deformations in which failure progresses slowly [1, 2]. In both cases, however, a reliable parameter is required to determine the fracture resistance of the structure of interest.

Fracture toughness is a measurement of fracture resistance [3] and is a crucial parameter in damage tolerance design and structural integrity assessment [4, 5]. Most safety-critical engineering structures including ships (see e.g., [6]) and offshore structures (see e.g., [7]) are manufactured from high (fracture) toughness materials[1] [8]. Stress intensity factor, J integral, crack-tip opening displacement, and crack tip opening angle are the most widely used concepts to evaluate fracture toughness [9, 10]. However, these experimental methods are expensive and time consuming [11] due to exhaustive specimen preparation, constant monitoring and rigorous data treatment, and difficulties in crack advance measurement [12]. Therefore, a straightforward, economical and reliable measurement of fracture toughness can accelerate the process and reduce costs.

Accurate measurement of fracture toughness requires a fatigue pre-cracked specimen which can be challenging to prepare in extremely brittle materials. Moreover, specimen thickness is another requirement which can be challenging to achieve as well, particularly in very tough materials. In addition, as crack tip constraints may have a strong effect on the laboratory measured values of fracture toughness [10, 13], technical development of an effective test methodology is necessary. Therefore, this article proposes a simple method, supported by physics-based analytical foundation, to accurately predict fracture toughness of metallic materials.

A simple method to predict fracture toughness has been interest of researchers. Researchers have attempted to correlate fracture toughness with tensile and microstructural properties of the material (see e.g., [14–17]. However, existing models are mainly based on empirical relationships and developed for (particular) ductile materials only. In the current article, on the

[1] High toughness does not necessarily correspond to ductility (see e.g., [3]).

other hand, a physics-based closed-form analytical expression is proposed to predict fracture toughness of both ductile and brittle materials. The expression naturally introduces a length scale parameter, consistent with the fact that fracture needs to be characterized over a microstructurally significant characteristic length [18, 19]. Hence, the proposed criterion can be incorporated into non-local computational methods, such as peridynamics [20–22] and other meshfree methods [23–25] as well thanks to the internal length scale parameter. In the current investigation, the proposed relationship is validated for a ductile and various brittle metallic materials.

The current research is verbally presented at ICSOS 2020 conference and this article encompasses extensive written presentation of it. The remainder of the article is organized as follows. Section 2 encompasses derivation of the analytical model, whereas Section 3 presents experimental validation of the model. Results are presented and discussed in Section 4, and conclusion remarks are given in Section 5.

2. Analytical Model

This section introduces the analytical models for brittle and ductile fracture of tensile mode for initially crack-free bodies. Tensile mode fracture corresponds to a crack formation with the plane of fracture having a normal in the direction of maximum principal stress. Representation of the potential fracture plane is shown in Figure 1.

2.1. Brittle Fracture

The derivation of the brittle fracture criterion is inspired by an energy balance concept, presented in a recent article [26]. The energy balance concept is based on continuum modeling of energy release rates, and it states that the system, seeking a minimum energy state, will fracture if the rate of energy change for the system in the fracture mode becomes less than that of the un-fractured continuum system. Therefore, the critical state is reached when the rate of energy change of the bulk system is balanced by the rate of energy change of the fractured medium.

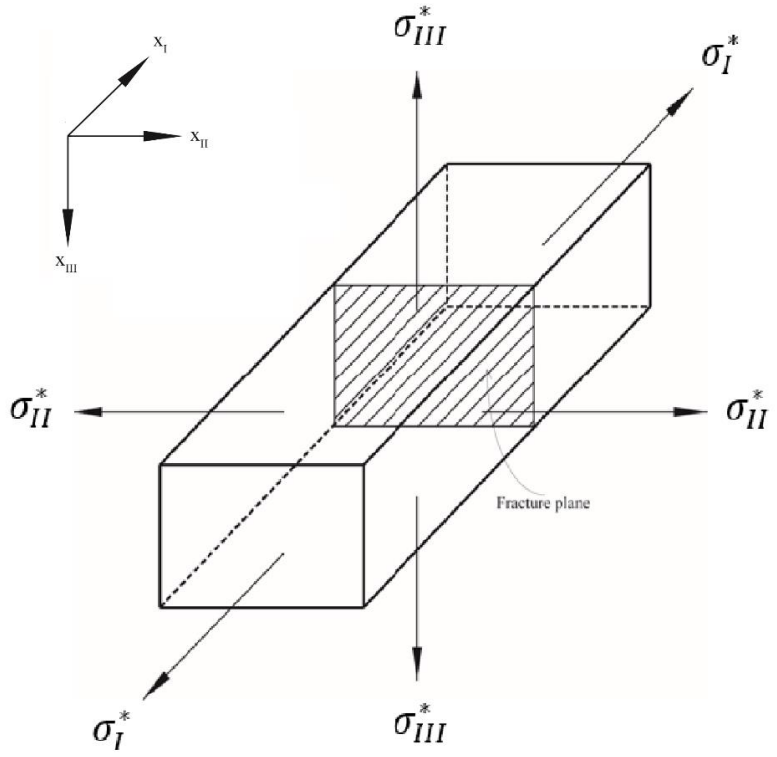

Figure 1 Volume element and the potential fracture plane (of tensile mode).

In the following, quasi-static loading conditions are applied and temperature changes are neglected. Moreover, the material is assumed to be homogeneous and isotropic, and remains within the elastic region. Accordingly, applying the energy balance concept by equating the rate of energy change of the un-fractured and fractured systems yields [27]

$$dW = (\Gamma_I \times A)de_I + dW^* \tag{1}$$

where dW and dW^* represent the total work increment for the unfractured and fractured systems, respectively. Also, de_I is the elastic strain increment in the first principal direction and A is the area of the fracture plane, which equals to $A = l_{II} \times l_{III}$. Moreover, Γ_I denotes necessary energy per unit area (per unit increment) to create new (fracture) surfaces, that is, critical effective energy release rate during the formation of new surfaces. In the case of pure brittle fracture, $\Gamma_I = 2\gamma_s$ as two (new) surfaces are created during fracture process. Here, γ_s represents surface energy per unit area.

Further simplification of Eq. (1) yields the critical state equation:

$$(1 + e_I)\sigma_I = \frac{\Gamma_I}{l_{I,0}} \tag{2}$$

where σ_I, e_I, and $l_{I,0}$ denote the maximum principal engineering stress, maximum principal engineering strain, and the characteristic length relevant to fracture process, respectively.

The critical state equation, i.e., Eq. (2), for a linear, isotropic material subjected to uniaxial tension simplifies into a quadratic equation in the form of

$$\sigma_I^2 + E\sigma_I - E\frac{\Gamma_I}{l_{I,0}} = 0 \tag{3}$$

where E denote the Young's modulus of the material. The positive root of Eq. (3) provides the tensile strength of the material of interest as

$$\sigma_{Ic} = -\frac{E}{2} + \sqrt{\frac{E^2}{4} + \frac{E\Gamma_I}{l_{I,0}}} \tag{4}$$

The global response of a system, e.g., toughness, strength, is often governed by the material behaviour at smaller length scales [28]. Therefore, length scale is an essential parameter in order to capture the non-classical material behaviour which usually appears at micro-scale [29, 30]. Natural existence of a length scale parameter (i.e., the characteristic length, $l_{I,0}$) enables Eq. (4) to be utilized in non-local computational methods. Rewriting Eq. (4) provides the characteristic length (relevant to fracture process)

$$l_{I,0} = \frac{E\Gamma_I}{\sigma_{Ic}^2 + E\sigma_{Ic}} \tag{5}$$

Additionally, characteristic length (relevant to fracture process) can be written in terms of Mode I plane strain fracture toughness, K_{Ic}, and the tensile strength, σ_{Ic}, as well, as in the following

$$l_{I,0} = \frac{(1-\upsilon^2)K_{Ic}^2}{\sigma_{Ic}^2 + E\sigma_{Ic}} \tag{6}$$

where υ denotes Poisson's ratio of the material.

Eq. (6) is obtained based on the assumption that critical energy dissipation (during the formation of new fracture surfaces) associated to initially crack-free bodies is equal to that of pre-cracked bodies. This is a reasonable assumption, as critical energy release rate is considered a material property (see e.g., [9]). Moreover, in fact, fracture initiation phenomena from a pre-crack system and a notched system are shown to be almost identical under tensile mode loading when the cleave plane is the same [31]. Accordingly, fracture initiation phenomena from a plain system, i.e., un-notched system, as well is believed to be almost identical to that of these two,

i.e., pre-crack system and notched system (T. Kitamura, personal communication at the ECF22 event, August 30th, 2018).

In the following, two special cases are investigated to expose the potential applications of the analytical model. The first one considers the case when Young's modulus and tensile strength are on the same order of magnitude (i.e., $\sigma_{Ic} = 0(E)$), whereas the second one considers the case when Young's modulus is much higher order of magnitude than the tensile strength (i.e., $E \gg \sigma_{Ic}$).

2.1.1. Special Case 1

Although it may not be of practical interest, mathematical interest triggers the evaluation of Eq. (5) for the upper limit case when Young's modulus and tensile strength are on the same order of magnitude. More precisely, let consider the case when tensile strength is equal to theoretical cohesive strength, that is, $\sigma_{Ic} = E/\pi$ [9]. In addition, pure brittle fracture is considered in which the critical effective energy release rate is expressed as $\Gamma_I = 2\gamma_s$. Thus, Eq. (5) in this case yields

$$\sigma_{Ic} = \sqrt{\frac{2E\gamma_s}{(1+\pi)l_{I,0}}} \approx \sqrt{\frac{E\gamma_s}{2l_{I,0}}} \tag{7}$$

Tensile strength given in Eq. (7) is consistent with the cohesive strength equation. Theoretical cohesive strength is given as [9]

$$\sigma_{cs} = \sqrt{\frac{E\gamma_s}{x_0}} \tag{8}$$

where x_0 is atomic spacing (at equilibrium). Therefore, the above analysis suggests that atomic spacing represents the characteristic length scale, i.e., $l_{I,0} \approx x_0/2$, when tensile strength is on the same order of magnitude of cohesive strength. This finding is consistent with Novozhilov's [32] study, where characteristic length dimension in the case of pure brittle fracture was shown to be equal to atomic radius. However, this analogy should be considered as a rough estimate, as the continuum assumption on which the current theory is based is not valid at the atomic scale.

2.1.2. Special Case 2

The second special case corresponds to practical cases, in which Young's modulus is approximately two to three times higher order of magnitude than the tensile strength (i.e., $E \gg \sigma_{Ic}$). Eq. (6) in this case yields

$$l_{I,0} \approx \frac{(1-\upsilon^2)K_{Ic}^2}{E\sigma_{Ic}} \tag{9}$$

Rewriting Eq. (9) provides the plane strain fracture toughness of material of interest as

$$K_{Ic} \approx \sqrt{\frac{l_{I,0}E\sigma_{Ic}}{1-\upsilon^2}} \tag{10}$$

2.2. Ductile Fracture

The aforementioned energy concept was utilized by Karr & Akçay [26] to determine ductile fracture locus. However, analytical concept proposed by Karr & Akçay [26] does not allow to predict fracture toughness of ductile materials. Therefore, here, the critical state equation derived in Section 2.1 is combined with the Equivalent Material Concept (EMC), proposed by Torabi [33], to derive a closed-form solution for fracture toughness of isotropic ductile materials.

The main idea of EMC is that a ductile material is equated with a virtual brittle material exhibiting linear elastic behavior. The EMC concept considers that the existing ductile material and the virtual brittle material have the same values of Young's modulus as well as the plane strain fracture toughness. Moreover, the strain energy density (i.e., the area under the stress-strain curve in uniaxial tension) of the existing ductile material is assumed to be equal to that of the virtual brittle material [33, 34].

Now consider a ductile material that obeys the power-law hardening relationship stated as

$$\Sigma = \Omega\varepsilon^{\mathrm{n}} \tag{11}$$

The power-law hardening relationship expressed by Eq. (11) can be utilized to describe most metals [35]. Here, Σ, ε, Ω, and n represent the true stress, true strain, hardening coefficient, and the hardening exponent, respectively, of the existing ductile material.

Equating strain energy densities of the existing ductile material (that obeys the aforementioned power-law hardening relationship) and the virtual brittle material with further simplification yields [33]

$$\sigma_{Ic}^{vb} = \sqrt{\left(\sigma_y^{ed}\right)^2 + \frac{2E\Omega}{n+1}\left[\left(\varepsilon_u^{ed}\right)^{n+1} - \left(\varepsilon_y^{ed}\right)^{n+1}\right]} \tag{12}$$

where σ_{Ic}^{vb} denote the tensile strength of the virtual brittle material. Moreover, σ_y^{ed}, ε_y^{ed}, ε_u^{ed} denote the yield strength, true strain at yield, and true strain at ultimate tensile strength, respectively, of the existing ductile material.

True strain at ultimate tensile strength (ε_u^{ed}) for a ductile material that obeys the power-law hardening relationship expressed by Eq. (11) is equal to hardening exponent of the material (n), i.e., $\varepsilon_u^{ed} = n$. Moreover, if the true strain at yield of the existing ductile material (ε_y^{ed}) is considered to be equal to 0.2% offset (which is commonly used to determine the yield strength of ductile materials), i.e., $\varepsilon_y^{ed} = 0.002$, Eq. (12) turns into

$$\sigma_{Ic}^{vb} = \sqrt{\left(\sigma_y^{ed}\right)^2 + \frac{2E\Omega}{n+1}\left[n^{n+1} - 0.002^{n+1}\right]} \tag{13}$$

On the other hand, plane strain fracture toughness of the virtual brittle material (K_{Ic}^{vb}) can be obtained utilizing Eq. (10) as

$$K_{Ic}^{vb} \approx \sqrt{l_{I,0}\frac{E\sigma_{Ic}^{vb}}{1-\upsilon^2}} \tag{14}$$

As the plane strain fracture toughness of existing ductile material is considered to be equal to that of virtual brittle material [33], Eq. (14) provides the plane strain fracture toughness of existing ductile material (K_{Ic}^{ed}) as well, that is, $K_{Ic}^{ed} = K_{Ic}^{vb}$. Therefore, plane strain fracture toughness of existing ductile material can be expressed by substituting Eq. (13) into Eq. (14)

$$K_{Ic}^{ed} \approx \sqrt{l_{I,0}\frac{E}{1-\upsilon^2}\sqrt{\left(\sigma_y^{ed}\right)^2 + \frac{2E\Omega}{n+1}\left[n^{n+1} - 0.002^{n+1}\right]}} \tag{15}$$

In fact, Eq. (14) and Eq. (15) can be utilized to predict the fracture toughnesses of not only ductile materials but also brittle materials. In other words, Eq. (15) reduces to Eq. (10) in the

case of a brittle material, as the tensile strength of virtual brittle material in Eq. (14), σ_{Ic}^{vb}, exchanges with that of existing brittle material, σ_{Ic}.

3. Materials and Methods

3.1. Materials

Two types of brittle materials and a ductile material are used for the validation of the analytical model presented above. A ductile material with small hardening coefficient is chosen to be consistent with the derivation of the analytical model. Experimental data of the materials of investigation are obtained from the open literature. As the experimental data on fracture of marine structural materials are scarce [36] and not sufficient to evaluate, only available material data in the open literature are considered in the current research.

3.1.1. Cast Iron

Recently, Han et al. [37] conducted experimental investigation on pearlitic graphite cast iron to study the effects of micro-structural factors on fracture toughness. The article investigated the fracture toughness of pearlitic graphite cast iron with six different nodularities. However, the current investigation considers the results of five cast iron samples, as the characteristic length of one sample cannot be interpreted from the reported results. The mechanical properties of these five cast iron samples are presented in Table 1.

As the cracks initiated at graphites [37], the characteristic length relevant to fracture process is taken as the average spacing between graphites. On the other hand, Young's moduli and Poisson's ratios of the cast iron samples were not reported by the authors. However, considering the Young's moduli and Poisson's ratios of similar cast irons, $E \approx 105$ GPa and $\upsilon \approx 0.18$ are used as representative values for the Young's moduli and Poisson's ratios of the cast iron samples of investigation.

Table 1 Mechanical properties of the cast iron samples [37].

Cast iron sample	Elongation (%)	$l_{I,0}$, μm	σ_{Ic}, MPa	K_{Ic}, $MPa\sqrt{m}$
G60N6	0.2	157	232	58±3
G62N6	0.5	144	268	64±5
G65N10	0.6	134	317	69±2
G87N18	0.7	74	356	40±2

G65N6	1.4	151	307	67±3

3.1.2. Metallic Glass

Experimental data of various metallic glasses are extracted from multiple sources and is compiled in Akçay [38]. The summary of the necessary data to predict the fracture toughness of metallic glasses are presented in Table 2. Interested readers on the original data sources are referred to Argon & Salama [39], Davis [40], Davis & Yeow [41], Davis [42], Nagendra et al. [43], Xi et al. [19], Yuan & Xi [44], Wang [45], and Madge et al. [46].

Table 2 Mechanical properties of the metallic glasses. See Akçay [38] for details.

Metallic glass	$l_{I,0}$, μm	σ_{Ic}, MPa	E, GPa	υ	K_{Ic}, $MPa\sqrt{m}$
$Ce_{60}Al_{20}Ni_{10}Cu_{10}$	5	600	30.3	0.313	10
$La_{55}Al_{25}Ni_5Cu_{10}Co_5$	~0.55	700	44.0	0.342	5
$Ni_{49}Fe_{29}P_{14}B_6Si_2$	0.38	2380	129.0	0.370	12
$Mg_{65}Cu_{25}Tb_{10}$	0.1	660	51.3	0.309	2

3.1.3. En3B Steel

Susmel & Taylor [47] investigated whether the Theory of Critical Distances (TCD) can predict failures in notched components when large plastic deformation exists. In this regard, they conducted experiments on notched En3B steel specimens. En3B steel has a yield strength of $\sigma_y = 606.2$ MPa, Young's modulus of $E = 197.4$ GPa, plane strain fracture toughness of $K_{Ic} = 97.4\, MPa\sqrt{m}$, hardening exponent of $n = 0.06$, and hardening coefficient of $\Omega = 882.7$ MPa [47]. However, the authors did not report any data on the dimple size or spacing between impurities. The only reported microstructural length feature of En3B steel by Susmel & Taylor [47] was the grain size, which was reported as 13 μm. Hence, considering the fact that grain size is correlated to the dimple size, a characteristic length of $l_{I,0} \approx 13$ μm is used in the current investigation. Poisson's ratio of En3B steel is taken as $\upsilon = 0.30$.

3.2. Methods

Fracture toughnesses of brittle materials (including the samples/materials exhibiting minor plastic deformation), i.e., cast iron samples and metallic glasses are predicted by Eq. (10),

whereas fracture toughness of the ductile material, i.e., En3B steel is predicted by Eq. (15). Results are presented and discussed in the following section.

4. Results and Discussion

Plane strain fracture toughness predictions for the cast iron samples are presented in Table 3. Although the application of the model is restricted up to small scale plasticity, fracture toughnesses of five different cast iron samples are determined to investigate the accuracy of the model at different (minor) plastic deformation levels. As can be seen from Table 3, the analytical model provides very good estimations except for G87N18 sample, which is the only sample that contains fine graphites. Although the exact reason for this high difference is not known, a fracture toughness within 3.0% deviation is obtained when the average size of graphites is used as a characteristic length rather than the average spacing of graphites.

Experimental plane strain fracture toughness data along with the analytical predictions for metallic glasses are presented in Table 4. Fracture toughness predictions for metallic glasses are in reasonably good agreement as well, with a maximum absolute relative error of 12.0%.

Table 3 Experimental data and analytical fracture toughness predictions for various cast iron samples. Experimental data are taken from Han et al. [37].

Cast iron sample	Experimental value, $MPa\sqrt{m}$	Analytical prediction, $MPa\sqrt{m}$	Absolute relative error (%)
G60N6	58	62.9	8.4
G62N6	64	64.7	1.1
G65N10	69	67.9	1.6
G87N18	40	53.5*	33.8*
G65N6	67	70.9	5.8

*Use of average size of graphites (instead of average spacing of graphites), which was reported as 39 μm by Han et al. [37], as a characteristic length yields a fracture toughness of 38.8 $MPa\sqrt{m}$ (corresponding to an absolute relative error of 3.0%).

Table 4 Experimental data and analytical fracture toughness predictions for various metallic glasses. See Akçay [38] for the details of the experimental data.

Metallic glass	Experimental value, $MPa\sqrt{m}$	Analytical prediction, $MPa\sqrt{m}$	Absolute relative error (%)
$Ce_{60}Al_{20}Ni_{10}Cu_{10}$	10	10.0	0.0
$La_{55}Al_{25}Ni_5Cu_{10}Co_5$	5	4.4	12.0
$Ni_{49}Fe_{29}P_{14}B_6Si_2$	12	11.6	3.3

$Mg_{65}Cu_{25}Tb_{10}$	2	1.9	5.0

Experimentally measured and analytically determined plane strain fracture toughness of En3B steel are presented in Table 5. Fracture toughness of En3B steel is determined as $K_{Ic} = 107.2$ $MPa\sqrt{m}$, which deviates 10.0% from the experimental value.

Table 5 Experimental datum and analytical fracture toughness prediction for a ductile metal. Experimental result is taken from Susmel & Taylor [47].

Metal type	Experimental value, $MPa\sqrt{m}$	Analytical prediction, $MPa\sqrt{m}$	Absolute relative error (%)
En3B steel	97.4	107.2	10.0

Fracture toughness predictions of materials of investigation are depicted in Figure 2 as well for illustration purposes. As the horizontal axis denotes the experimentally measured values and vertical axis denotes the predictions, the (black color) solid line corresponds to exact predictions. In other words, the amount of deviation from this line reflects the accuracy of the predictions. In this regard, the (red color) dashed lines encompass accurate predictions within 10% absolute relative error. Hence, the proposed method provides reasonably good estimations given the fact that even experimentally measured fracture toughness can exhibit considerable amount of scatter. However, additional experimental validations are needed, particularly for the ductile material application, to assure the accuracy of proposed method, as the validated data for ductile material application is restricted to only one material.

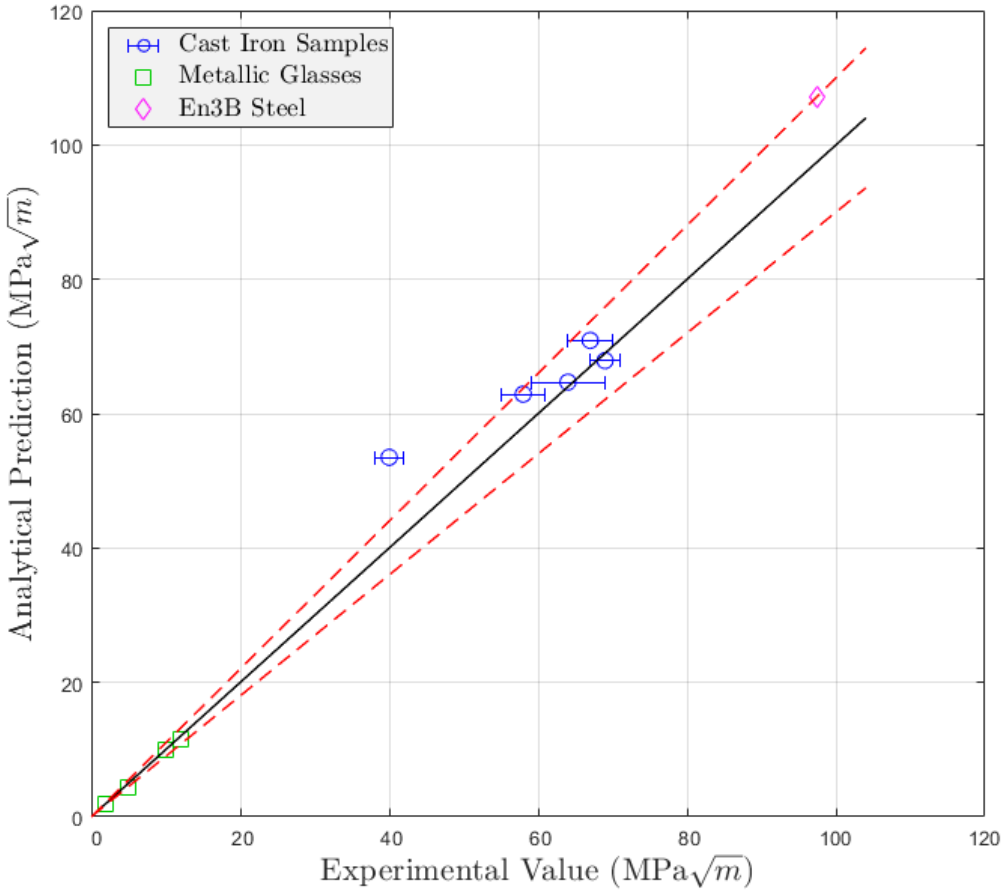

Figure 2 Accuracy of analytical predictions with respect to experimental data. The (black color) solid line corresponds to exact predictions, whereas the (red color) dashed lines encompass accurate predictions within 10% absolute relative error.

The use of EMC requires the yield strength and the ultimate tensile strength of the ductile material to be adequately close to each other, i.e., corresponding to a ductile material with small hardening exponent such that linear portion of the load-displacement curve during plane strain fracture toughness does not violate ASTM E399 standard [33]. Otherwise, experimentally measured plane strain fracture toughness does not correspond to a valid fracture toughness measurement [48]. Accordingly, as an alternative solution, recently, a modified version of EMC (called MEMC), in which a virtual fracture toughness is defined, is proposed and implemented by Torabi & Kamyab [48]. The current article implements the former concept, that is, the original EMC, which requires the use of low hardening (ductile) materials.

5. Conclusions

A physics-based closed-form expression is derived to predict plane strain fracture toughness of isotropic materials. The expression introduces a length scale parameter, an essential parameter in non-local computational methods, such as peridynamics. Moreover, use of the length scale

parameter, i.e., the characteristic length, as a mesh size removes mesh dependency in finite element applications. The proposed expression enables to predict fracture toughness of not only brittle materials but also ductile materials. The expression provides a faster and cheaper fracture toughness evaluation compared to the traditional methods, as it utilizes uniaxial tensile test results. Fracture toughness of two brittle materials (cast iron samples and various metallic glasses) and one ductile material (En3B steel) are predicted using the proposed expression. Fracture toughness of cast iron samples and various metallic glasses is determined to remain within 12% deviations except for G87N18 sample, whereas fracture toughness of En3B steel is determined to remain within 10% deviation. For G87N18 sample, which is the only sample that contains fine graphites, a fracture toughness within 3.0% deviation is obtained when the average size of graphites is used as a characteristic length rather than the average spacing of graphites.

Acknowledgement

This research is (partially) supported by Research Fund of Istanbul Technical University (Project ID: 41598).

Conflict of Interest

The authors declare no conflict of interest.

References

1. Orowan E (1945). Notch brittleness and the strength of metals. Transactions of the Institution of Engineers and Shipbuilders in Scotland 89:165–215.
2. Torabi AR. Berto F, Razavi SMJ (2018). Tensile failure prediction of U-notched plates under moderate-scale and large-scale yielding regimes. Theoretical and Applied Fracture Mechanics 97:434-439.
3. Ritchie RO (2011). The conflicts between strength and toughness. Nature Materials 10:817-822.
4. Li P, Cheng L, Yan X, Huang D, Qin X, Zhang X (2018). A temperature-dependent model for predicting the fracture toughness of superalloys at elevated temperature. Theoretical and Applied Fracture Mechanics 93:311-318.
5. Perez-Martin MJ, Erice B, Galvez F (2019). Experimental determination of the dynamic fracture-initiation toughness of high-strength metals. Engineering Fracture Mechanics 205: 498-510.
6. Wang YF, Wang LT, Jiang JC, Wang, J, Yang ZL (2020). Modelling ship collision risk based on the statistical analysis of historical data: A case study in Hong Kong waters. Ocean Engineering 197:106869.

7. Zhen X, Vinnem JE, Yang X, Huang Y (2020). Quantitative risk modelling in the offshore petroleum industry: Integration of human and organizational factors. Ships and Offshore Structures 15(1):1-18.
8. Launey ME, Ritchie RO (2009). On the fracture toughness of advanced materials. Advanced Materials 21:2103-2110.
9. Anderson TL (2005). Fracture mechanics: Fundamentals and applications. Boca Raton: CRC Press.
10. Zhu XK, Joyce JA (2012). Review of fracture toughness (G, K, J, CTOD, CTOA) testing and standardization. Engineering Fracture Mechanics 85:1-46.
11. Chen Z, Pan J, Jin T, Hong Z, Wu Y (2018). Estimation of fracture toughness of 16MnDR steel using Master Curve method and Charpy V-notch impact energy. Theoretical and Applied Fracture Mechanics 96:443-451.
12. Frómeta D, Lara A, Molas S, Casellas D, Rehrl J, Suppan C, Larour P, Calvo J (2019). On the correlation between fracture toughness and crash resistance of advanced high strength steels. Engineering Fracture Mechanics 205:319-332.
13. Doncheva E, Medjo B, Sedmak A (2015). Finite element analysis of fracture resistance parameters for stationary semi-elliptical surface cracks in high strength steel. Structural Integrity and Life-Integritet i Vek Konstrukcija 15:131-134.
14. Hahn GT, Rosenfield AR (1975). Metallurgical factors affecting fracture toughness of aluminum alloys. Metallurgical Transactions A 6:653-668.
15. Garrett GG, Knott JF (1978). The influence of compositional and microstructural variations on the mechanism of static fracture in aluminum alloys. Metallurgical Transactions A 9:1187-1201.
16. Gokhale AM, Deshpande NU, Denzer DK, Liu J (1998). Relationship between fracture toughness, fracture path, and microstructure of 7050 aluminum alloy: Part II. Multiple micromechanisms-based fracture toughness model. Metallurgical and Materials Transactions A 29:1203-1210.
17. Cvijović Z, Vratnica M, Rakin M (2006). Micromechanical modelling of fracture toughness in overaged 7000 alloy forgings. Materials Science and Engineering: A 434:339-346.
18. Ritchie RO, Knott JF, Rice JR (1973). On the relationship between critical tensile stress and fracture toughness in mild steel. Journal of the Mechanics and Physics of Solids 21:395-410.
19. Xi XK, Zhao DQ, Pan MX, Wang WH, Wu Y, Lewandowski JJ (2005). Fracture of brittle metallic glasses: Brittleness or plasticity. Physical Review Letters 94:125510.
20. Madenci E, Oterkus E (2014). Peridynamic theory and its applications. Springer: New York.
21. Javili A, Morasata R, Oterkus E, Oterkus S (2019). Peridynamics review. Mathematics and Mechanics of Solids, 24(11), 3714-3739.
22. Dai MJ, Tanaka S, Bui TQ, Oterkus S, Oterkus E (2021). Fracture parameter analysis of flat shells under out-of-plane loading using ordinary state-based peridynamics. Engineering Fracture Mechanics 244:107560.
23. Nguyen VP, Rabczuk T, Bordas S, Duflot M (2008). Meshless methods: A review and computer implementation aspects. Mathematics and Computers in Simulation 79(3):763-813.
24. Rabczuk T, Song JH, Zhuang X, Anitescu C (2020). Extended finite element and meshfree methods. Academic Press: London.

25. Liaghat F, Khosravifard A, Hematiyan MR, Rabczuk T (2021). An inverse procedure for identification of loads applied to a fractured component using a meshfree method. International Journal for Numerical Methods in Engineering 122(7):1687-1705.
26. Karr DG, Akçay FA (2016). A criterion for ductile fracture based on continuum modeling of energy release rates. International Journal of Fracture 197:201-212.
27. Akçay FA (2018). Theoretical prediction of fracture of initially crack-free brittle materials. Procedia Structural Integrity 13:1695-1701.
28. Budarapu PR, Rabczuk T (2017). Multiscale methods for fracture: A review. Journal of the Indian Institute of Science 97(3):339-376.
29. Wang B, Oterkus S, Oterkus E (2020). Determination of horizon size in state-based peridynamics. Continuum Mechanics and Thermodynamics. https://doi.org/10.1007/s00161-020-00896-y
30. Wang B, Oterkus S, Oterkus E (2020). Derivation of dual-horizon state-based peridynamics formulation based on Euler–Lagrange equation. Continuum Mechanics and Thermodynamics. https://doi.org/10.1007/s00161-020-00915-y
31. Huang K, Shimada T, Ozaki N, Hagiwara Y, Sumigawa T, Guo L, Kitamura T (2017). A unified and universal Griffith-based criterion for brittle fracture. International Journal of Solids and Structures 128:67-72.
32. Novozhilov VV (1969). On a necessary and sufficient criterion for brittle strength: PMM 33(2):212–222. Journal of Applied Mathematics and Mechanics 33(2):201-210.
33. Torabi AR (2012). Estimation of tensile load-bearing capacity of ductile metallic materials weakened by a V-notch: The equivalent material concept. Materials Science and Engineering: A 536:249-255.
34. Torabi AR (2017). Tensile failure in blunt V-notched ductile members: A new formulation of the equivalent material concept. Engineering Fracture Mechanics 184:1-13.
35. Yan S, Zhao X (2018). A fracture criterion for fracture simulation of ductile metals based on micro-mechanisms. Theoretical and Applied Fracture Mechanics 95:127-142.
36. Cerik BC, Park B, Park SJ, Choung J (2019). Modeling, testing and calibration of ductile crack formation in grade DH36 ship plates. Marine Structures 66:27-43.
37. Han SY, Sohn SS, Shin SY, Lee S, Suh YC (2013). In Situ fracture observation and fracture toughness analysis of pearlitic graphite cast irons with different nodularity. Metals and Materials International 19:673-682.
38. Akçay FA (2020). Structural characteristic length in metallic glasses. Journal of Mechanics 36(2):255-264.
39. Argon AS, Salama M (1976). The mechanism of fracture in glassy materials capable of some inelastic deformation. Materials Science and Engineering 23:219-230.
40. Davis LA (1979). Fracture toughnesses of metallic glasses. Metallurgical Transactions A 10:235-240.
41. Davis LA, Yeow YT (1980). Flow and fracture of a Ni-Fe metallic glass. Journal of Materials Science 15:230-236.
42. Davis LA (1986). Mechanical responses of metallic glasses. In Glass… Current Issues, Dordrech: Springer. p. 94-124.
43. Nagendra N, Ramamurty U, Goh TT, Li Y (2000). Effect of crystallinity on the impact toughness of a La-based bulk metallic glass. Acta Materialia 48:2603-2615.
44. Yuan CC, Xi XK (2011). On the correlation of Young's modulus and the fracture strength of metallic glasses. Journal of Applied Physics 109:033515

45. Wang WH (2012). The elastic properties, elastic models and elastic perspectives of metallic glasses. Progress in Materials Science 57:487-656.
46. Madge SV, Louzguine-Luzgin DV, Lewandowski JJ, Greer AL (2012). Toughness, extrinsic effects and Poisson's ratio of bulk metallic glasses. Acta Materialia 60:4800-4809.
47. Susmel L, Taylor D (2008). On the use of the Theory of Critical Distances to predict static failures in ductile metallic materials containing different geometrical features. Engineering Fracture Mechanics 75:4410-4421.
48. Torabi AR, Kamyab M (2019). Notch ductile failure with significant strain-hardening: The modified equivalent material concept. Fatigue & Fracture of Engineering Materials & Structures 42:439-453.